J Fluoresc (2017) 27:973–979
DOI 10.1007/s10895-017-2032-3

ORIGINAL ARTICLE

Microstructural and Radioluminescence Characteristics of Nd^{3+} Doped Columbite-Type $SrNb_2O_6$ Phosphor

Mete Kaan Ekmekçi[1] · Mustafa İlhan[2] · Arzu Ege[3] · Mehmet Ayvacıklı[3]

Received: 5 October 2016 / Accepted: 4 January 2017 / Published online: 13 January 2017
© Springer Science+Business Media New York 2017

Abstract Undoped and different concentration Nd^{3+} doped $SrNb_2O_6$ powders with columbite structure were synthesized by molten salt process using a mixture of strontium nitrate and niobium (V) oxide and NaCl-KCl salt mixture as a flux under relatively low calcining temperature. X-ray diffraction analysis results indicated that $SrNb_2O_6$ phases found to be orthorhombic columbite single phase for undoped, 0.5 and 3 mol% Nd^{3+} doping concentrations. Phase composition of the powders was examined by SEM-EDS analyses. Radioluminescence properties of Nd^{3+} doped samples from UV to near-IR spectral region were studied. The emissions increased with the doping concentration of up to 3 mol%, and then decreased due to concentration quenching effect. There is a sharp emission peak around 880 nm associated with $^4F_{5/2} \rightarrow {}^4I_{9/2}$ transition in the Nd^{3+} ion between 300 and 1100 nm. The broad emission band intensity was observed from 400 to 650 nm where the peak intensities increased by increasing Nd^{3+} doping concentration. All the measurements were taken under the room temperature.

Keywords Strontium metaniobate · Molten salt synthesis · Radioluminescence

✉ Mete Kaan Ekmekçi
mekmekci@marmara.edu.tr

[1] Department of Chemistry, Marmara University, Kadıkoy, 34777 Istanbul, Turkey

[2] Department of Materials Science and Engineering, Marmara University, Kadıkoy, 34777 Istanbul, Turkey

[3] Department of Physics, Celal Bayar University, 45140 Manisa, Turkey

Introduction

Optical and photonic technologies have an important act to play in developing new devices and leading to new innovations in increasing number of fields in industry and daily life. The photonic applications are used in several areas such as; optical data communications, bio-imaging, lighting and display technologies. Photonics also facilitates the human life producing new impressions and solutions in terms of speed, capacity and simplicity where today's technologies have nearly reached their limits. Rare earth doped oxide materials have excellent chemical and thermal stability along with outstanding luminescent efficiency and their color purity; consequently these are used for the various applications of display devices. Among the oxide materials, columbite-type niobate compounds [MNb_2O_6 (M = Sr, Co, Cd, Ni, Mg, Cu, Zn, Mn etc.)] having orthorhombic unit cell and space group Pbcn (60) [1, 2] are known as interesting host materials and they have remarkable interest due to their interesting optical, magnetic and dielectric properties [3–7]. The luminescence properties of metal niobates have been firstly reported by Watchel in 1960's [8]. There are several investigations on the luminescence properties of rare earth doped columbite niobates in the literature [9–15] whereas no studies exist on the radio luminescence properties of $SrNb_2O_6$.

The $SrNb_2O_6$ has an ordered columbite structure which consist of two SrO_6 and NbO_6 octahedras One of the advantage of this structure is to accept the guest ions easily which have similar ionic size with the existing metal and niobium ions. $SrNb_2O_6$ has an orthorhombic columbite structure with cell parameters a = 11.011 Å, b = 7.7136 Å, c = 5.5969 Å [16]. $SrNb_2O_6$ phase is used together with $BaNb_2O_6$ for the synthesis of $Sr_{0.53}Ba_{0.47}Nb_2O_6$ ceramics via the reactive sintering of $SrNb_2O_6$ and powders [17]. The solid solution of $SrNb_2O_6$ and $BaNb_2O_6$ has found many technological applications such

as electro-optic, pyroelectric, and piezoelectric devices. Ternary oxide $SrBi_2Nb_2O_9$ is one of the most promising candidates for lead-free non-volatile random access memory applications [18, 19]. $SrNb_2O_6$ nano rods have been hydrothermally synthesized as nano-structured high performance water-splitting photo catalyst [20].

There are several ways used to synthesize columbite niobates such as solid state [21], milling–annealing method [22], sol-gel combustion [23], coprecipitation [24], and electrochemical methods in the literature [25]. Nevertheless, due to some disadvantages of these methods make the molten salt method favorite in the synthesis of the niobates. In the wet chemical methods, generally require expensive and toxic organic-based compounds for synthesis of columbite niobate powders. Hydrothermal synthesis might be proper way lowering the synthesis temperature of niobates except that the heat treatment time is very long as 10 h. [26]. The co-precipitation technique will not work efficiently due to need of similar solubility of the cations which may led to different precipitate rate. For example, in the synthesis of $SrNb_2O_6$, both strontium and niobium can be precipitated simultaneously as oxalate and hydroxide compound at basic pH values. Sol- gel technique uses high prized raw materials as metal alkoxides compared to metal oxides and salts precursors and obtained products have weak mechanical properties. Moreover, using of the organic reagents in the synthesis may lead to carbon containing residue, particle agglomeration, poor control on particle morphology. There are also some disadvantages in traditional solid state reaction methods. The most encountered problems are inhomogeneity, poor nucleation and diffusion, high required sintering temperatures, undesired corundum-like ($A_4Nb_2O_9$) phase formations [27] and volatility of the reactant(s). The contaminations coming from crucibles and other containers are other unwanted problems in this method. The physical and chemical properties of ceramics are greatly affected by the characteristics of the powder in terms of particle size, morphology, purity and chemical composition [28]. The molten salt method can solve most of this problems with its easily application at lower synthesis temperatures with shorter dwell time giving a better chemical homogeneity, improved sintering ability and finer particle morphology than those produced by the solid state methods. Therefore, these features make the molten salt process a promising method. The molten salt method consist of incorporation of the stoichiometric amounts of metal oxides or metal salts together with the water soluble salt(s) system as a flux in an agat mortar by grinding to obtain homogenization of the powder mixture and needs proper heat treatment temperature and time to synthesize the desired material [29]. When compared molten salt technique to solid state reaction method, we achieved to synthesized undoped $SrNb_2O_6$ powders at 650 °C for 4 h than that of the solid state reaction at 1125 °C for 6 h in the literature [16].

In the present work, the phase formation, morphology and X-ray induced radioluminescence characteristics of undoped and $SrNb_2O_6$:Nd^{3+} powders synthesized by molten salt technique by avoiding poor compositional homogeneity, high sintering temperatures and prolonged reaction time have been studied and discussed.

Experimental

Undoped and 0.5, 3 and 6 mol% Nd^{3+} doped $SrNb_2O_6$ columbite ceramic powders were synthesized via molten salt route. For that reason, starting materials of strontium nitrate [$Sr(NO_3)_2$] and niobium oxide (Nb_2O_5) were taken in 6:1 salt to oxide weight ratio, while NaCl-KCl salt mixture was 1:1 in molar ratio. After that, neodymium oxide (Nd_2O_3) were added as a rare earth dopant and final powder mixture were ground and mixed well for the last time in agate mortar to provide further homogeneity. After calcination of the sufficient amount of mixture at 650 °C for 4 h in an alumina crucible, they were washed with ultra-pure water and vacuum filtered several times to remove ionic salts from the oxides. The presence of the sulphate ions in filtrate were checked by using qualitative reactions. After sintering process, the crystalline structures were characterized by X-ray diffractometer (XRD, Rigaku Corp., D-MAX 2200) using Cu-K_α radiation between 2θ = 15–65° at 2°/min and Ni filter. The morphology of the heat treated ceramic powders was investigated by Scanning Electron Microscopy (SEM, JEOL Ltd., JSM-5910LV) equipped with EDS (OXFORD Industries INCAx-Sight 7274; 133-eV resolution 5.9 keV) after Au-Pd coating.

RL spectrum of the undoped and Nd^{3+} doped phosphors were recorded in an X-ray unit with a Machlett OEG-50A tube operating with 30 kV and 15 mA. Luminescence detection system is conducted with a Horiba Jobin Yvon spectrometer, coupled to a liquid nitrogen cooled CCD detector. All RL spectrums were obtained between 300 and 1000 nm at room temperature with a detector integration time of 5 s. Input and output slit widths were adjusted to 2 mm. All the data presented here have been corrected for the spectral response of the system and are plotted in arbitrary units of intensity. All of the photoluminescence measurements were performed at room temperature.

Results and Discussions

X-Ray Diffraction Analysis

Figure 1 shows the XRD results of undoped and Nd^{3+} doped $SrNb_2O_6$ samples synthesized by using the NaCl:KCl salt system and 6:1 salt to oxide molar ratio with calcination time of 4 h at 650 °C. Both undoped and Nd^{3+} doped $SrNb_2O_6$

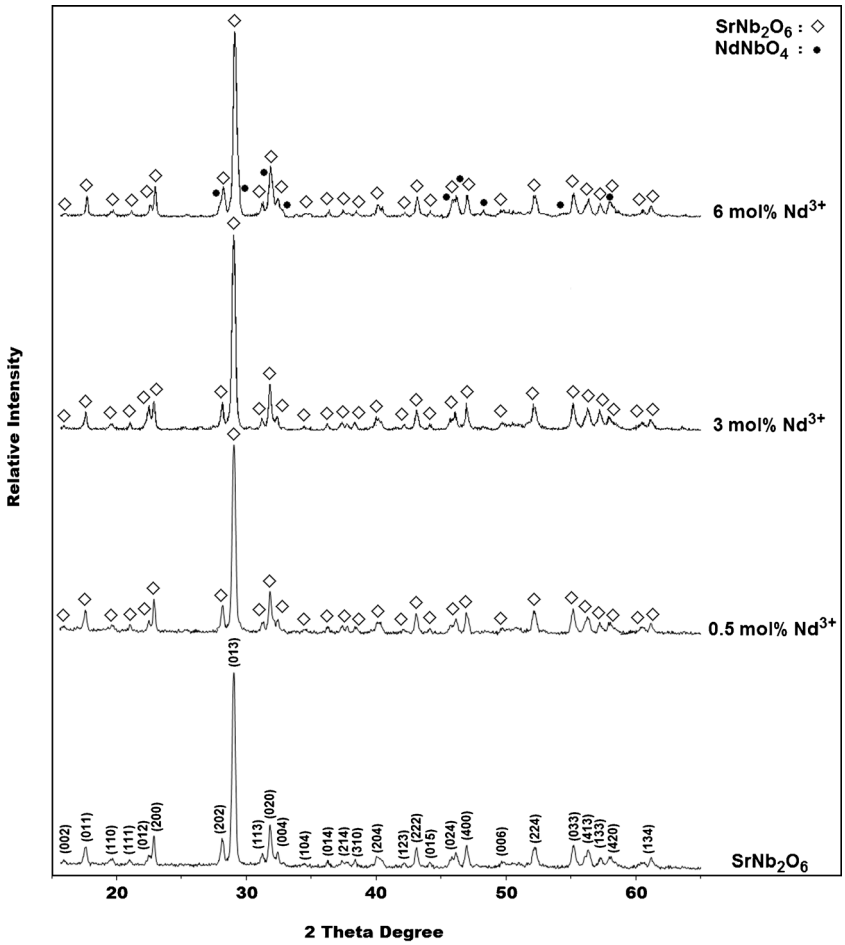

Fig. 1 XRD patterns of undoped $SrNb_2O_6$ (**a**), 0.5 (**b**), 3 (**c**) and 6 (**d**) mol% Nd^{3+} doped $SrNb_2O_6$ powders

phases crystallized (JCPDS card no: 28–1243) in orthorhombic symmetry with space group *Pbcn(60)* having the columbite type structure. Single phase has been determined for undoped 0.5 and 3 mol% Nd^{3+} doping concentrations, while $NdNbO_4$ (JCPDS card no: 32–0680) [30] minor phase has occurred for 6 mol% Nd^{3+} doping concentration.

In the columbite structure [31], there are three kinds of empty octahedral sites as *4a*, *4b* and *8d* in which the ion's radius and CN (coordination number) of Sr^{2+} (SrO_6) and Nb^{5+} (NbO_6) are 1.18 Å (for 6 C. N) and 0.64 Å (for 6 C. N) respectively [32]. Among the octahedral (*4a,4b,8d*) sites, when Nd^{3+} ions insert into *8d* sites, this may lead to a large repulsive force on adjacent Nb^{5+} ions. On the other hand, the *4b* sites are compressed due to the Jahn-Teller distortion of adjacent SrO_6 octahedral, while the *4a* sites are relatively free. The *4b* sites deformation would become relaxed if the Jahn-Teller Sr^{2+} cations disappear. Hence, based on the ion's radius and valence, the Nd^{3+} ions having an ionic radius of 0.983 Å (for 6 C. N) might occupy firstly *4a* and then *4b* sites up to 3 mol% doped concentration [31]. Also, Fig. 2 shows a shift to higher 2 theta angles for (013) peak depending on the Nd^{3+} concentrations. As expected, a decrease in lattice constant may be attributed to shrinkage of the lattice. These peak shifts

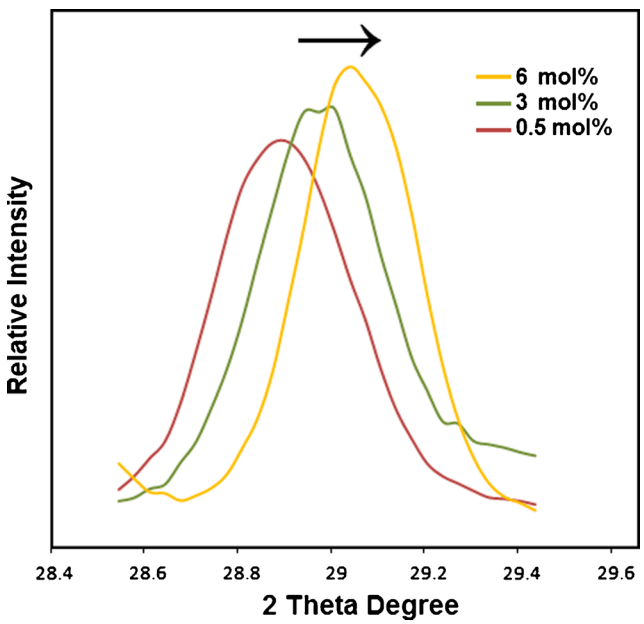

Fig. 2 Illustration of (013) peak shift to higher two theta angles depending on Nd^{3+} concentrations

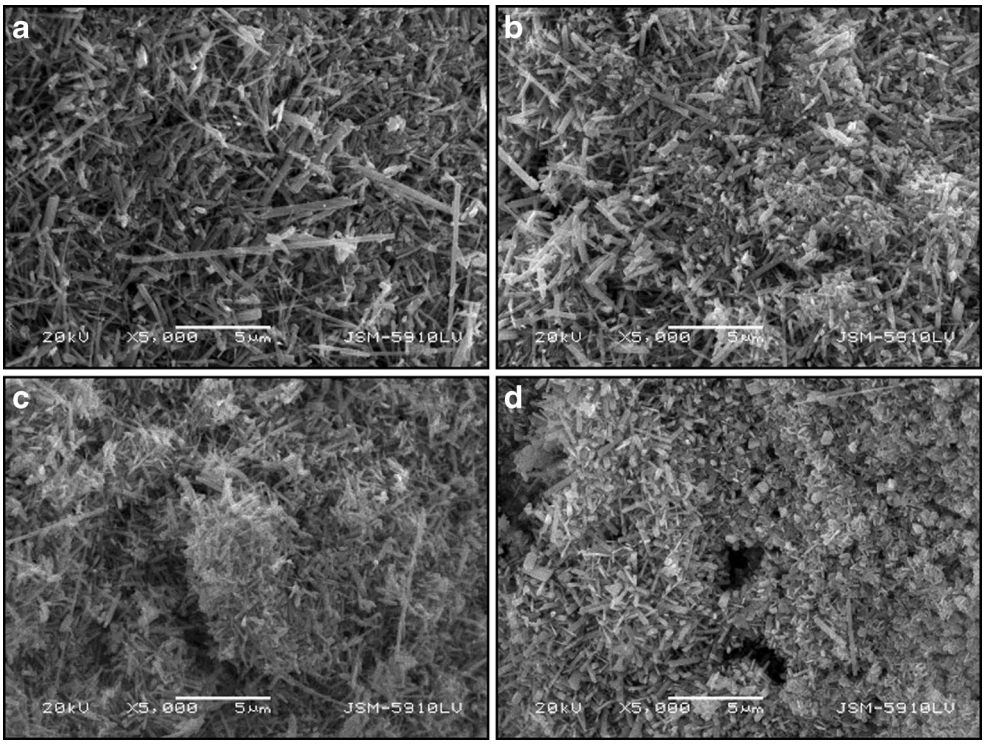

Fig. 3 Scanning electron microscopy (SEM) micrographs of undoped (**a**), 0.5 (**b**), 3 (**c**) and 6 mol% (**d**) Nd^{3+} doped $SrNb_2O_6$ structures

revealed the presence of strains in the doped host lattices. This situation indicated the successful location of Nd^{3+} ions in the lattice up to 3 mol%. Also, the incorporation of Nd^{3+} ions has caused a change in the phase structure of $SrNb_2O_6$ above

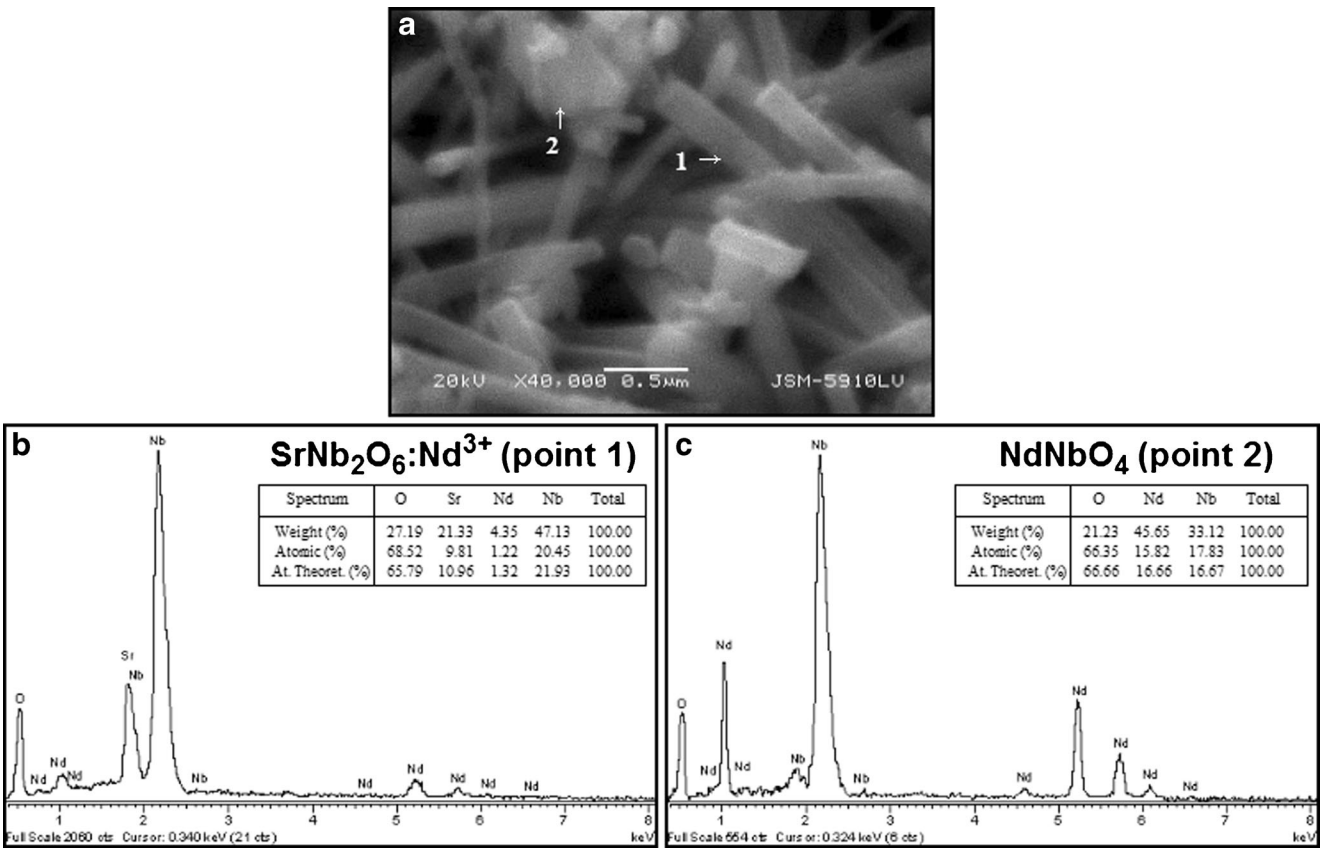

Fig. 4 SEM micrograph at 40.000× magnification (**a**), EDS spectra of 6 mol% Nd^{3+} doped $SrNb_2O_6$ structure (**b**) and $NdNbO_4$ secondary phase (**c**)

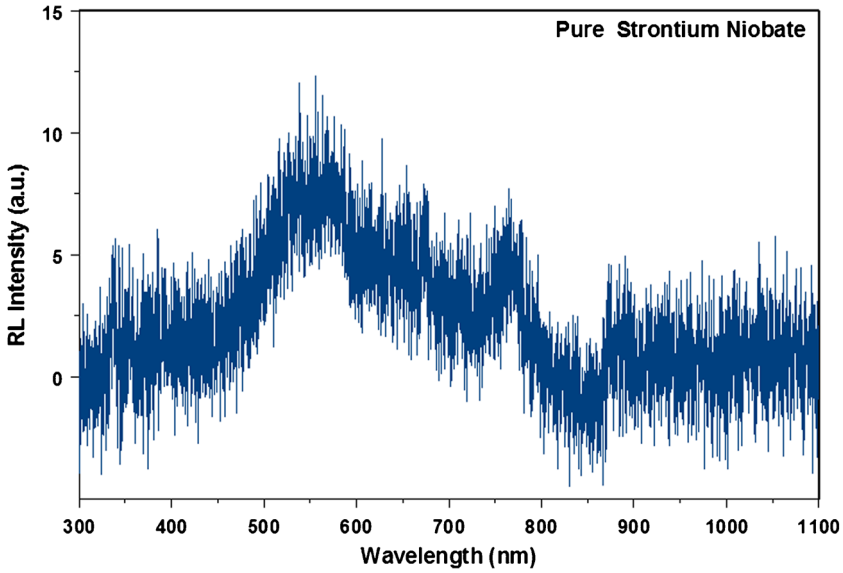

Fig. 5 The emission peak of $SrNb_2O_6$ host located around 550 nm under X-ray irradiation

3 mol% concentration. Accordingly, while Nd^{3+} ions occupied mostly the *4a*, and *4b* sites, a small amount of Nd^{3+} ions might have distorted the NbO_6 octahedral and led to the formation of $NdNbO_4$ secondary phase.

SEM-EDS Analysis

Figure 3a-d shows the SEM micrographs of undoped and Nd^{3+} doped powder samples at 5.000× magnification. The grains of undoped $SrNb_2O_6$ exhibited elongated shapes and grain sizes varied between 0.2 and 10 μm. Also, grain size of Nd^{3+} doped $SrNb_2O_6$ samples decreased by increasing dopant concentration. While grain size of the 0.5 mol% doped sample ranges between 0.2–5 μm, it was 0.1–2 μm for Nd^{3+} doped 6 mol% respectively. The decrease in grain size with increasing Nd^{3+} concentration may be attributed to the lattice distortion that suppressed the abnormality of grain growth. SEM and EDS investigations were also in agreement with the XRD results. SEM and EDS analyses also revealed differences in the elemental compositions between $SrNb_2O_6$ and $NdNbO_4$ grains. EDS analyses was performed at 20 kV of SEM acceleration voltage in order to detect the smaller grains present at surface. A SEM micrograph (Fig. 4a) at 40.000× magnification and EDS spectrums of 6 mol% Nd^{3+} doped samples were given in Fig. 4b,c. EDS analysis confirmed the Nd^{3+} doped $SrNb_2O_6$ presence (point 1 in Fig. 4b) and $NdNbO_4$ secondary phase detected (point 2 in Fig. 4c) having irregular shapes. The chemical compositions of both phases were in agreement with the theoretical compositions.

XRD and SEM-EDS results, some of the Nb^{5+} cation sites in $SrNb_2O_6$ structure may be distorted at 6 mol% doping concentration due to the presence of $NdNbO_4$ phase. Although

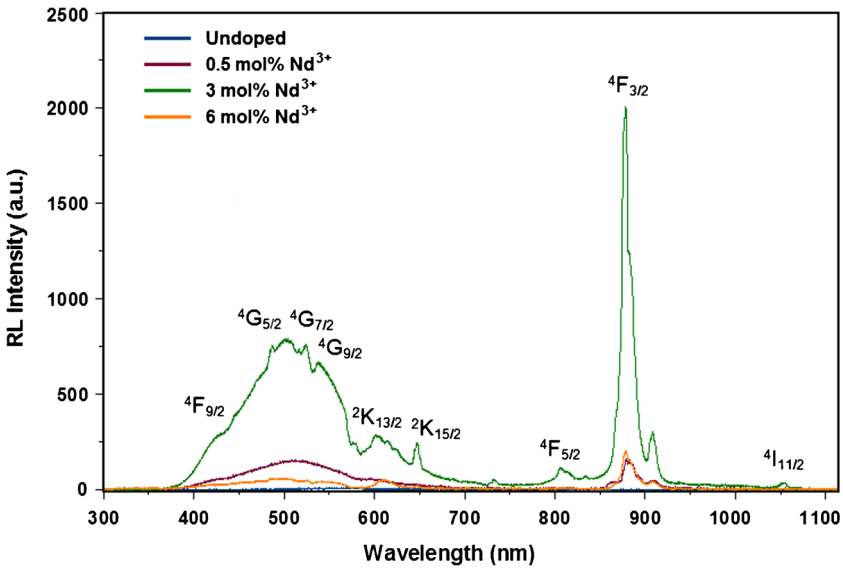

Fig. 6 The band transitions of undoped, 0.5, 3 and 6 mol% Nd^{3+} doped $SrNb_2O_6$ phosphors which correspond to $^4F_{9/2}$,$^4G_{5/2}$,$^4G_{7/2}$,$^4G_{9/2}$,$^2K_{13/2}$,$^2K_{15/2}$,$^4F_{5/2}$,$^4F_{3/2}$ and $^4I_{11/2} \rightarrow {}^4I_{9/2}$ under X-ray irradiation

the incorporation of Nd^{3+} ions will not have weight with the single phase structure of $SrNb_2O_6$ up to 3 mol% concentration, they will possibly affect the charge compensation due to increasing positive charges in the lattice.

Radioluminescence Analysis

Figure 5 shows the RL spectrum of $SrNb_2O_6$ host structure. A broad peak with weak intensity was observed between 300 and 800 nm. The excitation energy might be absorbed by SrO_6 and NbO_6 octahedrals of $SrNb_2O_6$ structure. However, the main luminescence features of $SrNb_2O_6$ host are defined by niobate group properties due to higher absorption of excitation energy [34]. As shown in the Fig. 5, the broad peak of the host located at 550 nm is due to transfer of absorbed excitation energy to the intrinsic NbO_6 groups of luminescence centers [33, 34]. The absorbed excitation energy may subsquently be transferred to the active centers of RE^{3+} ion in columbite structure.

Figure 6 shows the radio luminescence spectrums of 0.5, 3 and 6 mol% Nd^{3+} doped $SrNb_2O_6$ phosphors. There is a sharp an strong emission peak around 880 nm associated with $^4F_{5/2} \rightarrow {}^4I_{9/2}$ transition in the Nd^{3+} ion between 300 and 1100 nm. The broad emission band intensity was observed from 400 to 650 nm where the peak intensities increased by increasing Nd^{3+} doping concentration. In this energy transfer process, columbite lattice might have facilitated the absorption of excitation energy and its transfer to the dopant ions. The maximum emission intensity was obtained for the 3 mol% Nd^{3+} doped $SrNb_2O_6$ phosphor. From the RL spectra of Nd^{3+} doped $SrNb_2O_6$ phosphors, nine characteristic band pass emissions were observed as $^4F_{9/2} \rightarrow {}^4I_{9/2}$, $^4G_{5/2} \rightarrow {}^4I_{9/2}$, $^4G_{7/2} \rightarrow {}^4I_{9/2}$, $^4G_{9/2} \rightarrow {}^4I_{9/2}$, $^2K_{13/2} \rightarrow {}^4I_{9/2}$, $^2K_{15/2} \rightarrow {}^4I_{9/2}$, $^4F_{5/2} \rightarrow {}^4I_{9/2}$, $^4F_{3/2} \rightarrow {}^4I_{9/2}$ and $^4I_{11/2} \rightarrow {}^4I_{9/2}$, correspondingly to 421, 483, 525, 538, 601, 649, 808, 878 and 1060 nm respectively [35, 36]. It might be attributed that there is an energy transfer from columbite lattice to Nd^{3+} ions. On the other hand, emission intensity has sharply decreased for 6 mol% Nd^{3+} doped $SrNb_2O_6$. This may be ascribed to concentration quenching. The radioluminescence emission intensity increased with the increasing Nd^{3+} concentration of up to 3 mol%, and then decreased due to concentration quenching effect. Accordingly the quenching mechanism, two main factors could be considered as firstly, the presence of impurties and structural defects, and secondly, the critical distance between RE^{3+} ions [37, 38].

Conclusion

Undoped and Nd^{3+} doped $SrNb_2O_6$ crystalline powders were successfully synthesized by molten salt synthesis method at a relatively low temperature than that of the other traditional conventional methods. The spectroscopic properties of the Nd^{3+} ions in $SrNb_2O_6$ single crystal are reported. XRD analysis showed that undoped, 0.5 and 3 mol% Nd^{3+} doped powders were single phase with orthorhombic structure with the *Pbcn(60)* space group excluding the 6 mol% Nd^{3+} doped sample. SEM and EDS results are in agreement with the XRD findings. Radioluminescence measurements were performed between 300 and 1100 nm. The emission band peaking at 878 nm is found to be sharp which can be attributed to $^4F_{5/2} \rightarrow {}^4I_{9/2}$ transition of Nd^{3+}. The broad emission band intensity in the visible region was observed from 400 to 650 which are correspond to $^4F_{9/2}$, $^4G_{5/2}$, $^4G_{7/2}$, $^4G_{9/2}$, $^2K_{13/2}$ and $^2K_{15/2}$ energy levels. Also, RL results demonstrated three main bands in the near infrared region as $^4F_{5/2}$, $^4F_{3/2}$ and $^4I_{11/2}$ energy levels. The radioluminescence intensity increased up to 3 mol%, and then decreased due to concentration quenching effect. In this energy transfer process, columbite lattice might have facilitated the absorption of excitation energy and its transfer to the dopant ions.

References

1. Cummings JP, Simonsen SH (1970) The crystal structure of $CaNb_2O_6$. Am Mineral 55:90–97
2. Maeda M, Yamamura T, Ikeda T (1987) Dielectric characteristics of several complex oxide ceramics at microwave frequencies. Jpn J Appl Phys 26:76–79
3. Ballman AA, Porto SPS, Yariv AJ (1963) Calcium niobate $Ca(NbO_3)_2$-a new laser host. Appl Phys 34:3155
4. Greenblatt M, Wanklyn BM, Garrard BJ (1982) Flux growth of MNb_2O_6 (M = Mg, Zn, Ba) single crystals. J Cryst Growth 58: 463–466
5. Polgar K, Peter A, Paitz J, Zaldo C (1995) Crystal growth and preparation of colourless $MgNb_2O_6$ single crystals. J Cryst Growth 151:365–368
6. Heid C, Weitzel H, Burlet P, Winkelmann M, Ehrenberg H, Fuess H (1997) Magnetic phase diagrams of $CoNb_2O_6$. Physica B 574:234–236
7. Lee HJ, Hong KS, Kim SJ, Kim IT (1997) Dielectric properties of MNb_2O_6 compounds (where M = Ca, Mn, Co, Ni, OR Zn). Mater Res Bull 32:847
8. Wachtel A (1964) Self-activated luminescence of M21 niobates and tantalates. J Electrochem Soc 111:534–538
9. Zhou Y, Lü M, Qiu Z, Zhang A, Ma Q, Zhang H, Zhou G, Yang Z (2007) Photoluminescence characteristics of pure and Dy-doped $ZnNb_2O_6$ nanoparticles prepared by a combustion method. J Phys Chem C 111:10190–10193
10. Zhou R, Wei X, Huang S, Chen Y, Yin M (2012) Efficient near-infrared quantum cutting in Yb^{3+} doped $CaNb_2O_6$ phosphor based on energy transfer. J Alloys Compd 537:123–126
11. Cao J, Ji Y, Li J, Zhu Z, Wang Y, You Z, Tu C (2011) Crystal growth, Judd–Ofelt analysis and fluorescence properties of Tm^{3+}: $CaNb_2O_6$ crystal. J Lumin 131:1350–1354
12. De Camargo ASS, Silva RA, Andreeta JP, Nunes LAO (2005) Stimulated emission and excited state absorption in neodymium-doped $CaNb_2O_6$ single crystal fibers grown by the LHPG technique. Appl Phys B Lasers Opt 80:497–502

13. Camargo De ASS, Ferrari CR, Silva RA, Nunes LAO, Hernandes AC, Andreeta JP (2008) Spectroscopic features of erbium-doped CaM_2O_6 (M = Nb, Ta) single crystal fibers grown by the laser-heated pedestal growth technique. J Lumin 128:223–226
14. Mahlik S, Grinberg M, Kaminskii AA, Bettinelli M, Boutinaud P (2010) Luminescence of $Ca(NbO_3)_2$:Pr^{3+}: Pr^{3+} and self-trapped exciton emission. Radiat Meas 45:288–291
15. Pedrini C, Belsky A, Ivanovskikh KV, Petrosyan AG, Sargsyan RV, Kamenskikh I (2011) Cerium-, praseodymium- and terbium-trapped excitons in oxides. Chem Phys Lett 515:258–262
16. Singh KN, Bajpai PK (2011) Dielectric relaxation in pure columbite phase of $SrNb_2O_6$ ceramic material: impedance analysis. World Journal of Condensed Matter Physics 1:37–48
17. Lee WJ, Fang TT (1998) Nonisothermal reaction kinetics of $SrNb_2O_6$ and $BaNb_2O_6$ for the formation of $Sr_xBa_{1-x}Nb_2O_6$. J Am Ceram Soc 81:193–199
18. Leitner J, Hampl M, Růžička K, Straka M, Sedmidubský D, Svoboda P (2008) Thermodynamic properties of strontium metaniobate $SrNb_2O_6$. J Therm Anal Calorim 91:985–990
19. Leitner J, Hampl M, Růžička K, Sedmidubský D, Svoboda P, Vejpravová J (2006) Heat capacity, enthalpy and entropy of strontium bismuth niobate and strontium bismuth tantalate. Thermochim Acta 450:105–109
20. Chen D, Jinhua Y (2009) Selective-synthesis of high-performance single-crystalline $Sr_2Nb_2O_7$ nanoribbon and $SrNb_2O_6$ nanorod photocatalysts. Chem Mater 21:2327–2333
21. Pastor M, Goenka S, Maiti S, Biswas K, Manna I (2010) Phase evolution, dielectric and impedance spectroscopic study of $SrNb_2O_6$ columbite phase. Ceram Int 36:1041–1045
22. Huang T, Lin X, Xing J, Wang W, Shan Z, Huang F (2007) Photocatalytic activity of hetero-junction semiconductor WO_3/$SrNb_2O_6$. Mater Sci Eng B 141:49–54
23. Zhou Y, Ma Q, Lü M, Qiu Z, Zhang A, Yang Z (2008) Preparation and photoluminescence of $SrNb_2O_6$ nanoparticles prepared by combustion method. Mater Sci Eng B 150:66–69
24. Muthurajan H, Kumar HH, Rao NK, Pradhan S, Jha RK, Ravi V (2008) Low temperature synthesis of $SrNb_2O_6$ and $SrTa_2O_6$ using hydroxide precursor. Mater Lett 62:892–894
25. Fang J, Ma J, Sun Y, Liu Z, Gao C (2011) Electrochemical synthesis of nanocrystalline $SrNb_2O_6$ powders and characterization of their photocatalytic property. Mater Sci Eng B 176:701–705
26. Cho IS, Lee S, Noh JH, Kim DW, Jung HS, Kim DW, Hong KS (2010) Facile hydrothermal synthesis of $SrNb_2O_6$ nanotubes with rhombic cross sections. Cryst Growth Des 10(6):2447–2450
27. Ananta A, Brydson R, Thomas NW (1999) Synthesis, formation and characterisation of $MgNb_2O_6$ powder in a columbite-like phase. J Eur Ceram Soc 19:355–362
28. Natarajan N, Samuel V, Pasricha R, Ravi V (2005) A co-precipitation technique to prepare $BaNb_2O_6$. Mater Sci Eng B 117:169–171
29. Ekmekçi MK, Erdem M, Mergen A, Özen G, Bartolo BD (2014) Molten salt synthesis and spectral properties of Nd^{3+} doped $CdNb_2O_6$ columbite phosphors. J Alloys Compd 591:230–233
30. Zhao Y, Zhang P (2015) Phase composition, crystal structure, complex chemical bond theory and microwave dielectric properties of high-Q materials in a $(Nd_{1-x}Y_x)NbO_4$ system. RSC Advances Communıcatıon 118:193–198
31. Sato M, Hama YJ (1995) Lithium insertion characteristics of $CuNb_2O_6$. J Solid State Chem 118:193–198
32. Shannon RD (1976) Revised effective ionic radii and systematic studies of interatomic distances in halides and chalcogenides. Acta Crystallogr A32:751–767
33. Srivastava AM, Ackerman JF, Beeers WW (1997) On the luminescence of $Ba_5M_4O_{15}$(M = Ta^{5+}, Nb^{5+}). J Solid State Chem 134:187–191
34. Ayvacıklı M, Ege A, Ekdal E, Popovici EJ, Can N (2012) Radioluminescence study of rare earth doped some yttrium based phosphors. Opt Mater 34:1958–1961
35. Gordo VO, Arslanli YT, Canimoglu A, Ayvacikli M, Gobato YG, Henini M, Can N (2015) Visible to infrared low temperature luminescence of Er^{3+} and Nd^{3+}. Appl Radiat Isot 99:69–76
36. Dieke GH (1968) Spectra and energy levels of rare earth ions in crystals. Interscience Publishers, New York
37. Blasse G (1986) Energy transfer between inequivalent Eu^{2+} ions. J Solid State Chem 62:207–211
38. Garciá JS, Bausá LE, Jaque D (2005) An introduction to the optical spectroscopy of inorganic solids. John Wiley & Sons Ltd, England